Dalton Transactions

ROYAL SOCIETY OF CHEMISTRY

PAPER

View Article Online
View Journal | View Issue

Cite this: *Dalton Trans.*, 2025, **54**, 12189

Exploring zinc(II) ion binding and antimicrobial activity *via* D-amino acid substitution and *retro-inverso* modifications in MUC7 peptide from human saliva†

Joanna Wątły, *[a] Klaudia Szarszoń, [a] Arian Kola, [b,c] Fabio Zobi, [d] Tomasz Janek [e] and Daniela Valensin [b,f]

Received 7th March 2025,
Accepted 14th July 2025

DOI: 10.1039/d5dt00562k

rsc.li/dalton

Antimicrobial peptides are part of the host's innate immune response and have high therapeutic potential, especially in the complexes with Zn(II) ions. However, this potential is limited by poor proteolytic stability. To prevent this, their peptidomimetic modifications, such as D-amino acid substitution or *retro-inverso* strategy, are a worthy alternative. In this work, we investigate peptidomimetic modified fragments of MUC7, a protein present in human saliva, and their complexes with Zn(II) ions. A comprehensive analysis encompassing potentiometric titrations, far-UV circular dichroism and nuclear magnetic resonance spectroscopic techniques, mass spectrometry, density functional theory calculations, and biological assays revealed both similarities and distinctions compared to the native, non-modified peptide, offering valuable insights into the impact of sequence modifications on metal coordination, structural properties, and antimicrobial efficacy. This study is, to our knowledge, the first in-depth analysis of Zn(II) binding to *retro-inverso* peptides.

Introduction

The World Health Organization (WHO) has highlighted the growing threat of antibiotic-resistant bacterial strains to public health.[1] Antibiotic resistance is a global issue with significant economic consequences. The main contributors to antibiotic resistance include the excessive and prolonged use of antibiotics in human and veterinary medicine, as well as agriculture. These factors have accelerated the development and spread of drug-resistant microorganisms.[2]

Antimicrobial peptides (AMPs) are promising solutions to combat antibiotic resistance, displaying remarkable structural and functional diversity across organisms, from prokaryotes to humans. These peptides are crucial components of innate immune systems, providing an initial defense against pathogens.[3] Unlike traditional antibiotics, AMPs target multiple sites on bacterial membranes and intracellular structures, with some showing effectiveness against drug-resistant bacteria.[4] Both synthetic and natural AMPs demonstrate broad-spectrum antimicrobial activity with high specificity and low toxicity, making them strong candidates to counter antibiotic resistance.[5] Different types of AMPs, such as α-helical and β-sheet, bind to bacterial membranes in distinct ways, leading to changes in membrane structure. AMPs may cause membrane fragmentation or pore formation depending on their orientation in the membrane.[6]

Due to the essential role of divalent metal ions in bacterial and fungal survival and virulence, and considering the increasing prevalence of multi-drug resistant pathogens alongside the limited availability of new antibiotics, the exploration of novel therapies involving metal ions is gaining significant attention.[7] The coordination of metal ions can disrupt the balance of these metals in pathogens, potentially inhibiting their growth, while the direct cytotoxic effects of chelate complexes are also a major area of interest for scientific investigation.[8] Previous reports have shown that the antimicrobial activity of AMPs can be influenced by their interactions with metal ions such as Zn(II) and Cu(II), which may alter their modes of action either directly or indirectly.[9–16]

The relationship between metal cations and AMPs is commonly classified into three categories, each explaining

[a]*Faculty of Chemistry, University of Wrocław, F. Joliot-Curie 14, 50-383 Wrocław, Poland. E-mail: joanna.watly2@uwr.edu.pl*
[b]*Department of Biotechnology, Chemistry and Pharmacy, University of Siena, Via A. Moro 2, 53100 Siena, Italy*
[c]*Department Life Science, University of Siena, Via A. Moro 2, 53100 Siena, Italy*
[d]*Department of Chemistry, Fribourg University, Chemin Du Musée 9, 1700 Fribourg, Switzerland*
[e]*Department of Biotechnology and Food Microbiology, Wrocław University of Environmental and Life Sciences, Chełmońskiego 37, 51-630 Wrocław, Poland*
[f]*CIRMMP, Via Luigi Sacconi 6, 50019 Firenze, Italy*
† Electronic supplementary information (ESI) available. See DOI: https://doi.org/10.1039/d5dt00562k

different modes of action. This classification is based primarily on Zn(II) ions, which has provided substantial insight into their synergistic interactions: (i) Zn(II) directly modulates AMP activity by altering its charge or structure, either enhancing or inhibiting its antimicrobial effects; (ii) AMPs regulate Zn(II) availability, either by restricting its access to microbes (nutritional immunity) or increasing its intracellular concentration to toxic levels; (iii) Zn(II) can indirectly enhance AMP activity without forming a Zn(II)–AMP complex, such as by inhibiting bacterial SOS response mechanisms, thereby boosting DNA-targeting AMPs. Notably, these mechanisms can coexist, highlighting the complex bioinorganic interactions between Zn(II) and AMPs.[17–19]

The literature contains many examples of the synergistic role of Zn(II) ions in the antimicrobial activity of AMPs, *e.g.* shepherin I (Shep I), where Zn(II) binding to this peptide causes structural changes that lead to fibril formation, ultimately resulting in strong antifungal activity.[20] A similar mechanism of action was described for the Zn(II)–pramlintide complex.[21] Another noteworthy example of synergy was found between Zn(II) and histatin 5 (Hst5), a polyhistidyl peptide derived from human saliva, where the zinc ion acts as a 'switch' that inhibits the fungicidal activity of Hst5 in a concentration-dependent manner, preventing it from entering the *Candida albicans* cell and limiting its ability to kill the fungus.[22] Another interesting example is the clavanin family (antimicrobial peptides from *Styela clava*), particularly clavanin A (ClavA) and clavanin C (ClavC), whose activity is significantly enhanced by Zn(II). Zn(II) binding stabilizes ClavA's helical structure, strengthens its membrane interactions, and modifies membrane properties to facilitate bacterial penetration. At pH 7.4, ClavA disrupts membranes, whereas at pH 5.5, it interacts with DNA.[23,24] Our previous research on the peptide derived from the N-terminal 51-mer fragment of mucin 7 (MUC7) and its hydrolytic products (EGRERDHELRHRR and HHHQSPK) revealed that Zn(II) coordination significantly enhances antimicrobial activity against *Streptococcus sanguinis*, a commensal organism important in promoting oral health but capable of becoming pathogenic under certain conditions.[10,25]

The exploration of MUC7 peptides is increasingly recognized as a promising approach to combating bacterial and fungal infections, particularly in oral diseases. Notably, significant concentrations of Zn(II) ions in saliva (13.5 ± 12.2 μg L^{-1})[26] may enhance the antimicrobial activity of AMPs. The literature suggests that analogues designed to emulate the functional domains of MUC7 may enhance antimicrobial efficacy while helping to overcome microbial resistance.[27] However, AMPs (like all peptides) have one major drawback – they are susceptible to rapid enzymatic degradation, which limits their stability.[28] Therefore, designing peptidomimetics based on antimicrobial peptides is essential.[29] Such compounds offer a novel strategy for combating *e.g.* oral infections, which is especially relevant in light of growing concerns over antimicrobial resistance. These efforts represent a step toward developing more effective treatments for infections that are resistant to traditional antibiotics.

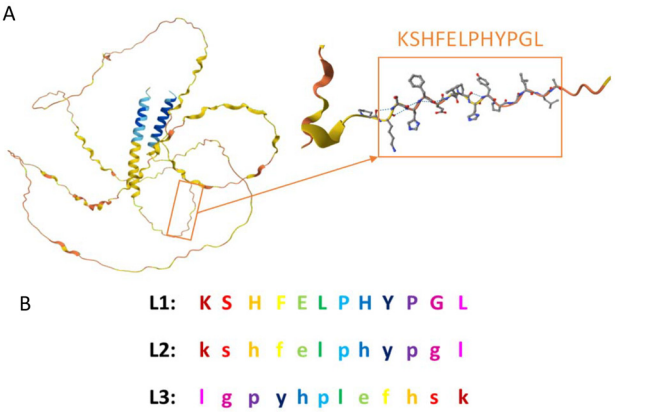

Fig. 1 (A) The AlphaFold-predicted structure of human MUC7 (UniProtKB: Q8TAX7) and a zoomed-in view of the studied peptide KSHFELPHYPGL (native sequence). (B) Schematic amino acid sequence representation of the 12-amino acid natural L-peptide, KSHFELPHYPGL, from the salivary protein MUC7 (L1) and its D-amino acid (L2) and *retro-inverso* (L3) peptidomimetics. Lowercase letters indicate D-amino acids.

In this work, we explore the influence of (i) D-amino acid substitutions and (ii) the *retro-inverso* (RI) modification on a 12-residue fragment of the human salivary peptide MUC7 (Fig. 1), with particular emphasis on their impact on Zn(II) coordination properties and antimicrobial activity. To improve proteolytic stability and enhance biological relevance, we selected analogues composed of D-amino acids, which are known to resist enzymatic degradation and, in some cases, exhibit enhanced receptor binding and biological efficacy.[30–33] Additionally, we employed the RI approach, which preserves the native side-chain topology while reversing the peptide backbone, thereby maintaining key molecular recognition features and further improving resistance to proteolysis.[34–36] A *retro* analogue composed of L-amino acids was not considered, as it lacks enzymatic stability and offers limited structural or functional advantage over the D- and RI-modified counterparts.

A comprehensive analysis is crucial for evaluating the coordination properties, thermodynamic stability, and structural characteristics of the native peptide (L1) and its peptidomimetic analogues (L2, L3). This approach enables the identification of both similarities and differences relative to the native peptide, providing insights into how sequence modifications influence coordination behavior, structural attributes, and antimicrobial activity.

Experimental

Materials

All the ligands (unprotected on C- and N-termini): KSHFELPHYPGL (L1), kshfelphypgl (L2), lgpyhplefhsk (L3) were purchased from KareBay Biochem (United States) (certi-

fied purity of 98%, Fig. S1†) and was used as received. In the trypsin digestion experiment, a 100 mM ammonium carbonate buffer was prepared by dissolving $(NH_4)_2CO_3$ (Chempur) in HPLC-grade water, adjusting the pH to 8.2 using a small amount of concentrated NaOH solution, and subsequently filtering the buffer. Trypsin from bovine pancreas (Merck) was dissolved in the same ammonium carbonate buffer. To terminate the reaction, trifluoroacetic acid (TFA; Fisher Scientific), diluted to 5% (v/v) in HPLC-grade water, was used. The samples for electrospray ionization-mass spectrometry (ESI-MS) were prepared using a mixture of ultrapure methanol (from Sigma-Aldrich) and water. $Zn(ClO_4)_2{\cdot}6H_2O$ was an extrapure product (Sigma-Aldrich). The concentrations of its stock solution was measured using inductively coupled plasma optical emission spectrometry (ICP-OES). The carbonate-free stock solution of 0.1 M NaOH (Eurochem) was standardized potentiometrically with potassium hydrogen phthalate (Sigma-Aldrich). The ionic strength (I) was adjusted to 0.1 M by addition of $NaClO_4$ (Sigma-Aldrich). All samples were prepared using freshly double-distilled water. For the EPR measurements, ethylene glycol (Chempur) was used. High-purity products for biological studies included 4-morpholineethanesulfonic acid (MES) and 4-(2-hydroxyethyl)piperazine-1-ethanesulfonic acid (HEPES), both sourced from Merck Millipore, Darmstadt, Germany. For the NMR experiments, deuterium oxide (99.90%, Cambridge Isotope Laboratories), 3-(Trimethylsilyl)propionic-2,2,3,3-d4 acid sodium salt (internal reference standard, Sigma-Aldrich), MES-d13 pH 5.4 (98%, Cambridge Isotope Laboratories) and phosphate buffer pH 7.4 (Sigma-Aldrich) were used. No human saliva or other human-derived biological samples were used.

Trypsin digestion experiment

Three samples, each containing 1 mg of the corresponding peptide: (1) KSHFELPHYPGL (L1), (2) kshfelphypgl (L2), and (3) lgpyhplefhsk (L3), were incubated with trypsin (5 mg mL^{-1}, 100 μL) in ammonium carbonate buffer (100 mM, pH 8.2, 900 μL) for 24 hours at 37 °C in a water bath. The reaction was quenched by the addition of 120 μL of trifluoroacetic acid (5% TFA) to lower the pH to approximately 3.5. The resulting mixture was transferred to Vivaspin 500 concentrators (PES membrane, 5000 Da), centrifuged, and analyzed using a JEOL JMS-S3000 SpiralTOF™-plus Ultra-High Mass Resolution MALDI-TOF MS with a cationic matrix (z = +1). A control sample containing only trypsin and buffer was prepared as a reference. The matrix solution was prepared using sinapic acid. Sinapic acid (10 mg) was dissolved in 1 mL of a 50 : 50 (v/v) acetonitrile/water solution containing 0.1% TFA. The sample and matrix were mixed in a 1 : 1 (v/v) ratio, spotted onto a 96-well stainless steel plate, and allowed to air dry. The results were analyzed using msTornado Analysis software (version 2.0.11.1).

Electrospray ionization-mass spectrometry (ESI-MS)

High-resolution mass spectra were obtained on a Bruker Compact QTOF (Bruker Daltonics) spectrometer equipped with an electrospray ionization source with an ion funnel. The instrument was operated in positive ion mode. The instrumental parameters were as follows: scan range m/z 50–3000; dry gas nitrogen; temperature 180 °C; capillary voltage 4000 V; ion energy 5 eV. The Zn(II) complexes [(metal : ligand stoichiometry of 1 : 1) $[ligand]_{tot} = 10^{-4}$ M] were prepared in a 50 : 50 MeOH/H_2O mixture. The samples were infused at a flow rate of 3 μL min^{-1}. The instrument was calibrated externally with the Low Concentration Tuning Mix ESI-ToF (Agilent Technologies). The data were processed using the Bruker Compass DataAnalysis 4.2 program.

Potentiometry

The pH-metric titrations were conducted in 0.004 M $HClO_4$ with an ionic strength of 0.1 M $NaClO_4$, utilizing a Metrohm Titrando 809 titrator and a Mettler Toledo InLab® Micro combined glass electrode. A thermostabilized glass cell, equipped with a magnetic stirring system, a microburet delivery tube and an inlet–outlet tube for argon was used for titrations. The solutions were titrated with 0.1 M carbonate-free NaOH. The electrode was calibrated daily for hydrogen ion concentration by titrating $HClO_4$ with NaOH in a total volume of 3.0 cm^3. The standard potential and the slope of the electrode couple were computed by means of the GLEE program.[37] Stability constants for proton and Zn(II) complexes were determined from titration curves performed over the pH range of 2–11 at a temperature of 25 °C in a total volume of 2.7 cm^3. The purities and exact concentrations of the ligand solutions were verified using the Gran method.[38] The ligand concentration was 0.4 mM, with a Zn(II) to ligand ratio of 0.8 : 1. Stability constant calculations and confirmation of the concentrations determined by the Gran method were carried out using the HYPERQUAD 2006 program.[39] Standard deviations were calculated using HYPERQUAD 2006 and accounted only for random errors. The constants for the hydrolysis Zn(II) ions were sourced from the literature.[40] The speciation and competition diagrams were generated using the HYSS program[41] and visualized with OriginPro 2016.

Nuclear magnetic resonance (NMR) spectroscopy

NMR spectra were recorded at 14.1 T using a Bruker Avance III 600 MHz spectrometer, using a 5 mm BBI (Broad Band Inverse) probe. The temperature was set and maintained to 298 K with an accuracy of ±0.1 K. The residual water signal was suppressed through excitation sculpting, employing a 2 ms selective square pulse on water. All samples were prepared in a mixture of 90% H_2O and 10% D_2O (99.90% purity from Cambridge Isotope Laboratories) with addition of deuterated MES-d13 20 mM buffer, pH 5.4 (Cambridge Isotope Laboratories) or phosphate 20 mM buffer, pH 7.4 (Sigma-Aldrich). 3-(Trimethylsilyl)propionic-2,2,3,3-d4 acid sodium salt (Sigma-Aldrich) was used as an internal reference standard. Proton resonance assignment was achieved using 2D ^1H–^1H total correlation spectroscopy (TOCSY) and nuclear Overhauser effect spectroscopy (NOESY) experiments, conducted with standard pulse sequences. Data processing and analysis were completed using the Bruker TOPSPIN 3.6.5

program. The samples of the analyzed complexes were prepared by adding $Zn(ClO_4)_2$ (at different Zn(II)/L molar ratios) to solutions of a 0.5 mM ligand in appropriate buffer, followed by adjusting the pH to 5.4 and 7.4, as needed. The NMR spectra recorded both in the presence and absence of metal ion identified specific metal-binding sites, and the combination of all methods used provided insights into the coordination geometries.

Density functional theory (DFT) calculations

All calculations were carried out using the Gaussian 09 software. Geometry optimizations and frequency analyses were conducted in water using the B3LYP functional,[42,43] paired with the 6-31G(d,p) basis set. For the Zn(II) ion, the default spin formalism was applied, and default Gaussian 09 values were used for numerical integration grids, SCF, and geometry optimization convergence criteria. No symmetry constraints were applied during the geometry optimizations. The nature of the stationary points was confirmed by computing vibrational frequencies to ensure they were true minima. The relative energies of the peptide-bound $[L\#Zn(H_2O)_2]^+$ species and the N-terminus-bound complexes were calculated by considering thermochemical data from the Gaussian output and adopting the free energies of reaction changes ($\Delta_r G^\circ$):

$$\Delta_r G^\circ\,(298.15\,\mathrm{K}) = \sum (\varepsilon_0 + G_{\mathrm{corr}})_{\mathrm{products}} - \sum (\varepsilon_0 + G_{\mathrm{corr}})_{\mathrm{reactants}}$$

where ε_0 = total energy of the molecule and G_{corr} = Gibbs free energy correction, for the following general reaction:

$$[ZnHL1\text{-}NH_2]^+\{2N_{His},\ 2H_2O\} \rightarrow [ZnHL1]^+\{2N_{His}, 1H_2O, 1NH_2\} + H_2O$$

where {*n*X} indicates the number *n* of residues or molecules bound to Zn(II), and NH_2 refers to the deprotonated N-terminal amino group. All energies are given in kJ mol^{-1}.

In vitro antimicrobial activity of peptides and peptide–metal ion systems

The antimicrobial properties of three peptides and their metal complexes were evaluated against several pathogenic strains that affect humans. This included four reference strains obtained from the American Type Culture Collection (ATCC), specifically *Escherichia coli* ATCC 25922, *Pseudomonas aeruginosa* ATCC 15442, *Enterococcus faecalis* ATCC 29212, and *Staphylococcus aureus* ATCC 25923. Additionally, two strains from the Polish Collection of Microorganisms (PCM) were tested: *Streptococcus mutans* PCM 2502 and *Streptococcus sanguinis* PCM 2335, along with *Candida albicans* SC5314, used for antimicrobial activity testing.[44] *E. coli* ATCC 25922, *P. aeruginosa* ATCC 15422, *E. faecalis* ATCC 29212, and *S. aureus* ATCC 25923 were grown at 37 °C in Mueller-Hinton broth (MHB) supplied by Merck Millipore (Darmstadt, Germany). *S. mutans* PCM 2502 and *S. sanguinis* PCM 2335 were cultured in Brain Heart Infusion (BHI) broth, also from Merck Millipore (Darmstadt, Germany), and incubated anaerobically (85% N_2, 10% H_2, and 5% CO_2) overnight at 37 °C. *C. albicans* SC5314 was grown aerobically at 37 °C in Yeast Peptone Dextrose (YPD) broth from A&A Biotechnology (Gdańsk, Poland).

Bacterial susceptibility assay

The minimal inhibitory concentrations (MICs) of the peptides/complexes were assessed by employing the serial broth microdilution technique.[45] In brief, two-fold serial dilutions of each peptide/Zn(II) complex (1 : 1 molar ratio) were prepared in MHB, BHI, and YPD broth, each buffered with either 10 mM MES (pH 5.4) or 10 mM HEPES (pH 7.4) (both from Merck Millipore, Darmstadt, Germany) in volumes of 100 μL in 96-well flat-bottom microtiter plates (Sarstedt, Nümbrecht, Germany). The final concentrations of the peptides/complexes ranged from 7.8 to 500 μg mL^{-1}. Each well was inoculated with 1 μL of a 24-hour microorganism culture, resulting in a final cell density of 5×10^7 CFU mL^{-1}. Negative control and growth control wells did not contain the tested compounds. Zn(II) ion (10 μg mL^{-1}) served as negative control, as it exhibited no antimicrobial effects. Additional controls included bacteria and *C. albicans* incubated with metal ions. The microplates were incubated for 24 h at 37 °C for *E. coli* ATCC 25922, *P. aeruginosa* ATCC 15422, *E. faecalis* ATCC 29212, *S. aureus* ATCC 25923 and *C. albicans* SC5314. Two oral bacteria strains, *S. mutans* PCM 2502 and *S. sanguinis* PCM 2335 were incubated anaerobically at 37 °C (85% N_2, 10% H_2, and 5% CO_2) and OD_{600} was measured after 72 h using a microplate reader (Spark®, Tecan Trading AG, Switzerland). The MIC endpoint was determined as the lowest concentration that led to complete (100%) inhibition of growth. All assays were conducted in triplicate.

Results and discussion

Enzymatic stability

Trypsin digestion experiments were conducted to evaluate the proteolytic stability of the native peptide L1 and its peptidomimetic analogues L2 and L3. The L1 peptide, composed entirely of L-amino acids, was readily cleaved by trypsin, as evidenced by a characteristic fragment signal observed in the MALDI mass spectrum (m/z = 1296.62, Fig. S2†). In contrast, both L2 (containing all D-amino acids) and L3 (a *retro-inverso* analogue, also composed of D-amino acids) remained intact under identical conditions, with no detectable cleavage products observed. These findings confirm that substitution with D-amino acids, as well as application of the *retro-inverso* strategy, effectively enhances resistance to enzymatic degradation.

Ligand deprotonation

Table 1 presents the deprotonation constants (pK_a) of the native peptide (L1) and its peptidomimetic analogues (L2 and L3) along with their likely assignments to specific chemical groups. For the L2 peptide, the deprotonation constant of the C-terminus was not determined, as it likely deprotonated at a lower pH, beyond the standard operating range of the electrode. Consequently, only six pK_a values were determined. All

Table 1 Deprotonation constants (pK_a) for L1, L2 and L3 peptides[a] and stability constants (log β) for their complexes with Zn(II) ions in aqueous solution of 4 mM $HClO_4$ with I = 0.1 M $NaClO_4$ at 25 °C. C_L = 0.4 mM; molar ratio M : L – 0.8 : 1. The standard deviations are reported in parentheses as uncertainties on the last significant figure

KSHFELPHYPGL (L1)				kshfelphypgl (L2)				lgpyhplefhsk (L3)			
Species	log β_{jk} [b]	pK_a [c]	Residue	Species	log β_{jk} [b]	pK_a [c]	Residue	Species	log β_{jk} [b]	pK_a [c]	Residue
$[H_7L]^{4+}$	47.47(4)	2.91	COOH	$[H_7L]^{4+}$	—	—	COOH	$[H_7L]^{4+}$	48.22(3)	3.01	COOH
$[H_6L]^{3+}$	44.56(2)	3.82	Glu	$[H_6L]^{3+}$	46.70(3)	3.99	Glu	$[H_6L]^{3+}$	45.21(2)	3.98	Glu
$[H_5L]^{2+}$	40.74(2)	5.98	His	$[H_5L]^{2+}$	42.71(3)	6.21	His	$[H_5L]^{2+}$	41.23(1)	6.18	His
$[H_4L]^{+}$	34.76(1)	6.72	His	$[H_4L]^{+}$	36.50(3)	6.89	His	$[H_4L]^{+}$	35.05(1)	6.83	His
$[H_3L]$	28.04(2)	7.55	H_3N^+	$[H_3L]$	29.61(2)	8.78	H_3N^+	$[H_3L]$	28.22(1)	7.81	H_3N^+
$[H_2L]^{-}$	20.49(1)	9.78	Tyr	$[H_2L]^{-}$	20.83(1)	10.07	Tyr	$[H_2L]^{-}$	20.41(1)	9.72	Tyr
$[HL]^{2-}$	10.71(1)	10.71	Lys	$[HL]^{2-}$	10.76(2)	10.76	Lys	$[HL]^{2-}$	10.69(1)	10.69	Lys
Zn(II) complexes											
	log β_{jk} [d]	pK_a [e]			log β_{jk} [d]	pK_a [e]			log β_{jk} [d]	pK_a [e]	
$[ZnH_2L]^{+}$	24.73(2)			$[ZnH_2L]^{+}$	26.65(4)			$[ZnH_2L]^{+}$	25.71(1)		
[ZnHL]	17.20(2)	7.53		[ZnHL]	18.20(4)	8.45		[ZnHL]	18.35(2)	7.36	
								$[ZnL]^{-}$	8.86(3)	9.49	
$[ZnH_{-1}L]^{2-}$	−2.17(4)			$[ZnH_{-1}L]^{2-}$	−1.59(5)			$[ZnH_{-1}L]^{2-}$	−1.23(2)	10.09	
								$[ZnH_{-2}L]^{3-}$	−12.20(3)	10.97	

[a] The deprotonation constants of the ligands reported herein were determined to support both our previously published study[52] and the present work. [b] Constants are presented as cumulative log β_{jk} values. $\beta(H_jL_k) = [H_jL_k]/([H]^j[L]^k)$, in which [L] is the concentration of the fully deprotonated peptide. [c] pK_a values of the peptides were derived from cumulative constants: $pK_a = \log\beta(H_jL_k) - \log\beta(H_{j-1}L_k)$. [d] Zn(II) stability constants are presented as cumulative log β_{ijk} values. L stands for a fully deprotonated peptide ligand that binds Zn(II) ion: $\beta(M_iH_jL_k) = [M_iH_jL_k]/([M]^i[H]^j[L]^k)$, where [L] is the concentration of the fully deprotonated peptide. [e] $pK_a = \log\beta(M_iH_jL_k) - \log\beta(M_iH_{j-1}L_k)$.

of the obtained pK_a constants are typical values found in a variety of similar peptides and proteins.[10,21,46–51] Fig. S3† presents the species distribution diagrams for the studied peptide and its peptidomimetics. When comparing the studied ligands, a noticeable difference in the pK_a value of the N-terminus (greater by more than one unit) was observed for the L2 peptide in contrast to the native (L1) and *retro-inverso* (L3) peptides. We performed DFT calculations to investigate the relative spatial arrangement and stability of the protonation states of peptides L1 and L2 in water, aiming to better understand the observed pK_a differences. The qualitative trends in the relative free energies of protonated *versus* deprotonated species provided valuable insight. Structurally, we observed that L1 adopts a more compact and stable conformation in water across different protonation states, whereas L2 remains more extended and flexible (Fig. S4†). In the N-terminus deprotonation step, the energy required to deprotonate L2 is ∼211 kJ mol^{-1} higher than that for L1, implying that the deprotonated species $[H_3L1]$ is significantly more stable than $[H_3L2]$. This matches the experimental finding that L1 exhibits a lower N-terminal pK_a in the $[H_3L]$ state. While the structures of the peptides alone do not fully explain the observed pK_a shifts, the combined influence of geometry and relative stabilization energies provides a coherent and mechanistically plausible explanation for the differing pK_a values observed between L1 and L2. The deprotonation constants of the ligands reported herein were determined to support both our previously published study[52] and the present work.

Zn(II) – MUC7 fragments – insight into coordination properties

The characterization of Zn(II) complexes was performed using electrospray ionization mass spectrometry (ESI-MS) to confirm the stoichiometry of complexes formed in solution, potentiometry (to determine stability constants and construct competition plots), nuclear magnetic resonance (NMR) spectroscopy (to identify donor atoms), and Far-UV circular dichroism (to analyze secondary structure of peptide before and after Zn(II) coordination). Additionally, DFT calculations were performed to confirm the experimental results.

The ESI-MS results (Table S1 and Fig. S5–S7†) indicate that all of the peptides form a monomeric complex species with the Zn(II) ion under given conditions, neither poly-nuclear complexes nor bis-complexes were observed. The strongest signals (m/z) for each system were identified and matched to their respective species. The alignment between the experimental and simulated spectra, including signal intensities and isotopic patterns, confirms the correctness of the interpretation. Additional signals found in the spectra mainly represent sodium and potassium adducts of the ligands and complex species, along with residual impurities from the measuring instrument.

Based on a series of potentiometric titrations, the stability constants of Zn(II) complexes were calculated using previously reported hydrolysis constants for zinc from the literature.[40] The resulting stability constants are presented in Table 1. The corresponding distribution diagrams of complex species are presented in Fig. 2. For Zn(II)–L1 and Zn(II)–L2 systems, three distinct complex species were identified in solution at pH range of 5.5–11, while for Zn(II)–L3, five complex species were detected.

The proposed coordination modes of Zn(II) ion in these complexes are discussed below.

Zn(II)–L1 (KSHFELPHYPGL) system

The first complex detected in solution is $[ZnH_2L]^+$, which begins to form at pH 5.5 and reaches its maximum concen-

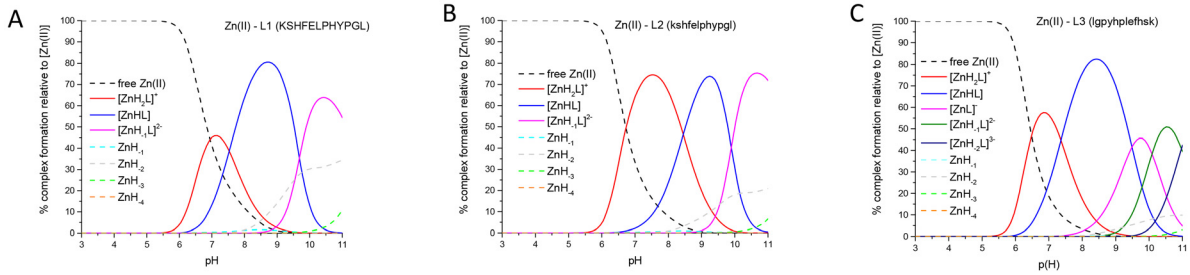

Fig. 2 Representative distribution diagram for (A) Zn(II)–L1 (KSHFELPHYPGL); (B) Zn(II)–L2 (kshfelphypgl) and (C) Zn(II)–L3 (lgpyhplefhsk) systems in aqueous solution of 4 mM $HClO_4$ with I = 0.1 M $NaClO_4$ dependent on pH values. C_L = 0.4 mM; molar ratio M : L – 0.8 : 1. Dashed lines indicate free Zn(II) ions and the curves corresponding to Zn(II) hydrolysis.

tration at pH 7.1 (Fig. 2A). Based on a series of potentiometric titrations, it can be suggested that the Zn(II) ion is coordinated by the imidazole nitrogen atoms of the two His residues in the sequence. At this pH, deprotonation and binding of the N-terminal amino group or deprotonation of a water molecule within the Zn(II) coordination sphere are also likely to occur.

The subsequent complex species, [ZnHL], reaches its maximum concentration at pH 8.7 and has a pK_a value of 7.53. Its formation is likely associated with: (i) deprotonation of the non-coordinating N-terminal amino group (pK_a = 7.55), provided it was not involved in Zn(II) binding in the previous species, or (ii) deprotonation of a water molecule. The final detected complex species, $[ZnH_{-1}L]^{2-}$, reaches its maximum concentration at pH 10.4 and is formed through the simultaneous deprotonation of the Tyr and Lys residues in the ligand, suggesting an unchanged coordination mode.

To gain more insight into the zinc binding modes, mainly at pH 5.4 and 7.4 (pH values important for balance in the human oral cavity), NMR analyses were conducted. Prior to assessing the effects of the metal ion, the NMR assignments of the peptide protons were obtained by using standard 2D ^1H–^1H TOCSY and NOESY experiments. As expected, at physiological pH, most NH signals were very considerably broadened, apart from Ser2 and Phe4 NH signals, which disappeared completely. Furthermore, the peptide exhibited no significant NOE correlations indicating a lack of specific structuring in aqueous solution.

Upon the addition of increasing amount of zinc (0.25–1.00 equivalents), no effects were evident at pH 5.4, strongly indicating the absence of Zn(II)–L1 association at acidic pH, which is also in agreement with the potentiometric results. However, the broadening and chemical shift variations were observed in selected proton resonances at pH 7.4. The most significant changes in the NMR spectra were found for the Lys1 Hα and His3/His8 Hε signals, which shifted downfield by 0.02–0.03 ppm in the presence of 1.0 equivalent of Zn(II) (Fig. 3, left panel). Furthermore, subtle variations were observed in residues near the two His residues (Glu5, Leu6 and Pro7). These findings strongly support the coordination of Zn(II) to the N-terminal amino group and two imidazole nitrogen atoms from two His residues in both $[ZnH_2L]^+$ and [ZnHL]

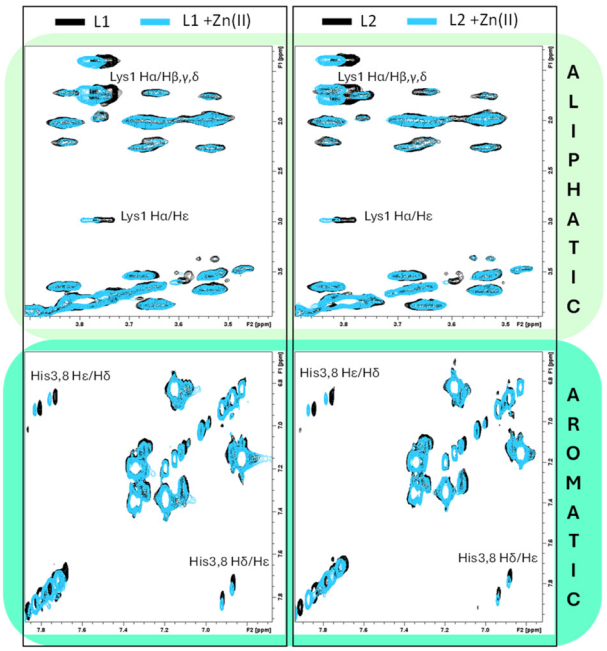

Fig. 3 Comparison of selected regions of NMR ^1H–^1H TOCSY spectra of L1 (KSHFELPHYPGL) and L2 (kshfelphypgl) (black contours) and in presence of 1.0 Zn(II) eqs. (light blue contours). [L1] = [L2] = 0.5 mM, T = 298 K, pH 7.4, 20 mM phosphate buffer.

complex species at pH 7.4 (Fig. 2A), suggesting $\{2N_{im}, -NH_2\}$ and $\{2N_{im}, -NH_2, 1OH^-\}$ coordination modes, respectively. Additionally, the effects observed on the His Hε signals indicate that Nδ, rather than Nε, is the preferred imidazole nitrogen involved in the metal coordination sphere.

DFT calculations are in support of our assignment (Fig. S8†). Starting at pH 5.5, the $[ZnH_2L]^+$ species is best described by the Zn(II) ion coordinated to the two His residues in the sequence, with Nδ binding preferred over Nε coordination by *ca.* 67 kJ mol^{-1}. In addition, the calculations suggest that deprotonation of the N-terminal amino group is favored over a deprotonated Zn(II)-coordinated water molecule (*i.e.* a Zn(II)–OH^- species) by *ca.* 59 kJ mol^{-1}. Following deprotonation of the N-terminal amino group, water displacement and N-terminus coordination to Zn becomes possible. The result-

ing $[ZnH_2L]^+$ $\{2N_{im}, -NH_2\}$ peptide complex is *ca.* 88 kJ mol^{-1} higher in energy than the $[ZnH_2L]^+$ $\{2N_{im}, OH^-\}$ species. This relative increase in energy may be attributed to the decrease in number of internal degrees of freedom of the molecule associated, *e.g.*, to bond rotations in the chelate $\{2N_{im}, -NH_2\}$ peptide complex.

Zn(II)–L2 (kshfelphypgl) system

The potentiometric results for the Zn(II) complexes with the D-amino acid analogue are very similar to those observed for the Zn(II)–L1 system and strongly suggest the same coordination modes for all complex species present in solution (Table 1 and Fig. 2B). The NMR spectra for the L2 peptide were also very similar to those of L1, with only small variations in the His and Lys1 residues (data not shown). Consistently, upon the addition of increasing amounts of zinc (0.25–1.00 equivalents) to L2, broadening and chemical shift variations were observed at pH 7.4, with no noticeable effects at pH 5.4. The most significant changes were seen for the Lys1 Hα and His3/His8 Hε signals, which mirrored the behavior observed with L1 (Fig. 3 and Fig. 4). These results indicate that Zn(II) binding mode is maintained in both L1 and L2, regardless of the presence of D or L amino acids. This observation was also confirmed by the theoretical DFT calculations (Fig. S8†).

Zn(II)–L3 (lgpyhhplefhsk) system

This system is characterized by the presence of a greater number of complex species within the studied pH range in the potentiometric measurement compared to the Zn(II)–L1 and Zn(II)–L2 systems (Table 1 and Fig. 2C). The first complex species detected in solution is $[ZnH_2L]^+$, which dominates at pH 6.9. Potentiometric data strongly suggest that this complex involves a $\{2N_{im}\}$ donor set and one additional deprotonation, originating either from (i) a water molecule coordinated to Zn (II) or (ii) the N-terminal amino group of the peptide. The appearance of the subsequent complex species, [ZnHL], which reaches maximum concentration at pH 8.4, may also result from similar deprotonation events – either of a water molecule or the N-terminus (if not previously coordinated). Theoretical calculations confirm that, unlike the Zn(II)–L1 and Zn(II)–L2 systems where N-terminal amino group deprotonation is preferred over deprotonation of a Zn-bound water molecule, in Zn (II)–L3 the two differ by only 3 kJ mol^{-1}, with the latter giving a lower energy system. The obtained pK_a values do not precisely indicate when the Zn(II) ion binds to the amino group (analogously to the above-described systems with Zn(II) ions), but they strongly support its involvement in zinc coordination in the $[ZnH_2L]^+$ or [ZnHL] complex species. However, analogously to what theoretically observed for the L1 and L2 systems, following deprotonation of the N-terminal amino group, water displacement and N-terminus coordination to Zn(II) is possible for L3, resulting in a $[ZnH_2L3]^+$ $\{2N_{im}, -NH_2\}$ peptide complex *ca.* 96 kJ mol^{-1} higher in energy than the $[ZnH_2L3]^+$ $\{2N_{im}, -OH^-\}$ species.

The presence of another complex species, $[ZnL]^-$, with a pK_a value of 9.49, is associated with the deprotonation of an additional water molecule in the metal's coordination sphere resulted in $\{2N_{im}, 2OH^-\}$ donor set. Above pH 10, deprotonation of non-coordinating Tyr residue (pK_a = 10.09 for the complex and pK_a = 9.72 for the free ligand) and Lys residue (pK_a = 10.97 complex and pK_a = 10.69 for the free ligand) occurs, leading to the formation of two next complex species: $[ZnH_{-1}L]^{2-}$ and $[ZnH_{-2}L]^{3-}$.

NMR spectroscopy is consistent with L1 and L2, Zn(II) binding does not occur at pH 5.4, as no changes were observed in the spectrum. However, the addition of Zn(II) ions to L3 at pH 7.4 resulted in greater broadening of NMR signals compared to the L1 and L2 systems (Fig. S9† and Fig. 5). The effects induced by Zn(II) coordination are more pronounced in peptide L3, as evidenced by the substantial broadening of its NMR signals upon metal addition. In contrast, peptide L2 exhibits only moderate line broadening; however, the observed chemical shift variations, particularly in the histidine residues, are consistent with Zn(II) coordination *via* imidazole nitrogens. These differences reflect variations in the exchange regime

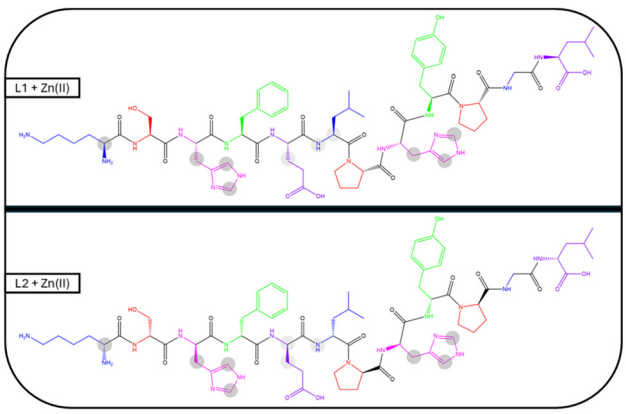

Fig. 4 Schematic representations of the NMR effects observed on Zn(II) complexes with L1 and L2 systems. The gray circles indicate nuclei that are more significantly affected by Zn(II) ions, as determined from 1D and 2D NMR spectra at physiological pH.

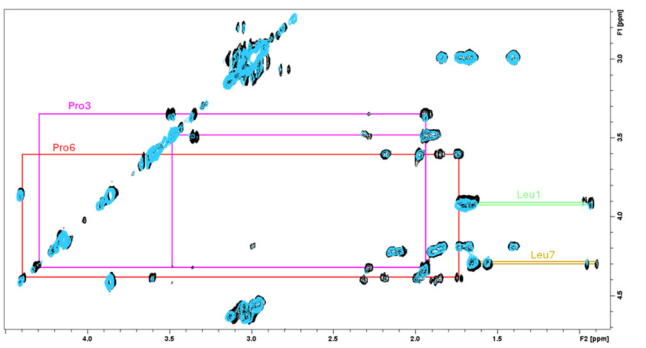

Fig. 5 Comparison of the aliphatic regions of NMR ^{1}H–^{1}H TOCSY spectra of L3 (lgpyhplefhsk) alone (black contours) and in presence of 1.0 Zn(II) eqs. (light blue contours). [L3] = 0.5 mM, T = 298 K, pH 7.4, 20 mM phosphate buffer.

between the L2 and L3 systems, rather than differences in binding affinity, as Zn(II) is diamagnetic.

Specifically, our data indicate that, in addition to the slight shifts observed in the aromatic protons of His5/His10 and the Hα signals of Leu1/Leu7 (suggesting the same coordination mode for the Zn(II) ion as in L1 and L2), several residues, including Pro3, Tyr4, Pro6, and Phe9, exhibited decreased signal intensity in the presence of Zn(II). Notably, the aromatic protons of Phe4 and Tyr9 were the most affected (Fig. S9†).

Furthermore, analysis of the NOESY spectra of the Zn(II)–L3 complex revealed NOEs between the aromatic protons of Phe and His (Fig. 6). As shown in the figure, His Hε exhibits dipolar interactions with all the aromatic protons of Phe9, while His10 Hδ correlates only with Phe9 Hε and Hζ.

These interactions, observable only in the NOESY spectra recorded in the presence of Zn(II), strongly suggest the proximity of the His and Phe aromatic rings, possibly interacting through π–π stacking. Once again, theoretical calculations are in full support of the proximity of the His10 and Phe9 residues, with the aromatic hydrogens being separated in space by a distance in a range as low as 4.5–5 Å (Fig. 7).

These interactions may additionally stabilize the Zn(II)–L3 complex, which is reflected in the competition plot (Fig. 8) by the highest affinity of Zn(II) ions for L3 ligand. However, a close analysis of the DFT coordination environment of Zn(II) in the three systems suggests that the higher stability of the Zn(II)–L3 complex may be also assigned to the stabilization of coordination geometry of the Zn(II) ion. This is nearly perfectly tetrahedral with L3, but subjected to higher strain in L2 and L1, as exemplified by the values of angle θ, defined by $N\delta_{His}$–Zn(II)–$N\delta_{His}$, in the coordination sphere of the metal ion (Fig. 7 and 8).

Additionally, DFT calculations indicate that coordination *via* the terminal $-NH_2$ group is energetically less favorable, yet NMR spectroscopy demonstrates its occurrence in solution. This apparent contradiction can be rationalized by the local peptide environment: only the Tyr side chain flanks the binding site, whereas the Phe residue – positioned between the two His residues – is sterically displaced upon Zn(II) coordination to the imidazole rings. As illustrated for ligands L1 and L2 (Fig. S10†), and in agreement with previous computational studies,[53] Zn(II) does not migrate to the carboxylate terminus – shielded by Tyr – but instead reorients by simple C–N bond rotation at the amino terminus, enabling direct $-NH_2$ coordination.

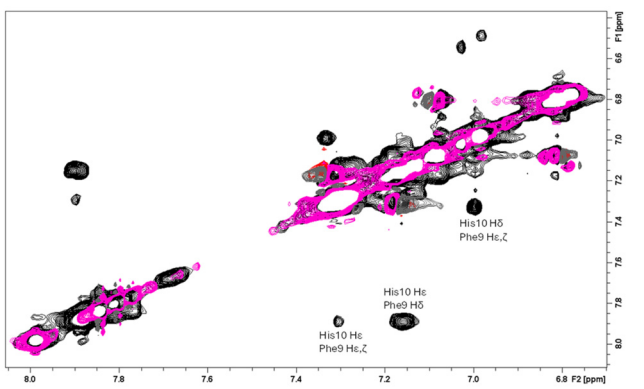

Fig. 6 Comparison of the aromatic regions of NMR ^1H–^1H NOESY spectra of L3 (lgpyhplefhsk) alone (black contours) and in presence of 1.0 Zn(II) eqs. (magenta contours). [L3] = 0.5 mM, T = 298 K, pH 7.4, 20 mM phosphate buffer.

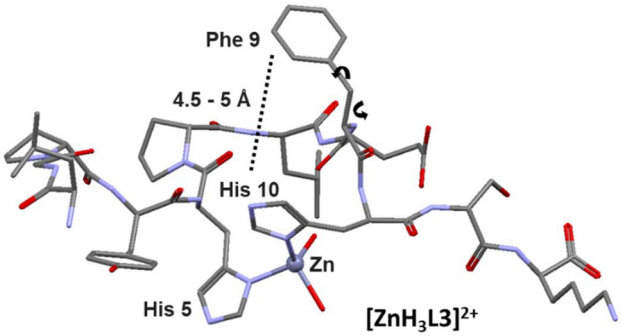

Fig. 7 DFT optimized $[ZnH_3L3]^{2+}$ structure, highlighting the proximity of the His10 and Phe9 residues. The minimum distance between the aromatic hydrogens of the residues (4.5–5 Å) was calculated as a function of the rotation of the benzyl group of Phe9. At pH 7.4, the proximity of these two residues is only observed in the calculated Zn(II)–L3 system, and in both $[ZnH_3L3]^{2+}$ and $[ZnH_2L3]^{+}$ complex species.

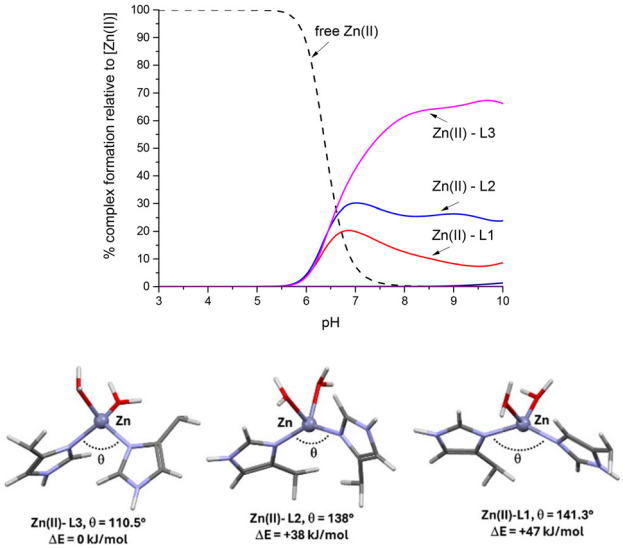

Fig. 8 Top: competition plot between L1 (KSHFELPHYPGL), L2 (kshfelphypgl) and L3 (lgpyhplefhsk) with Zn(II) ions describing complex formation at different pH values in a hypothetical situation, in which equimolar amounts of the all reagents are mixed. Conditions: T = 298 K, [Zn(II)] = [L1] = [L2] = [L3] = 0.001 M. Bottom: calculated coordination environment of the Zn(II) ion in the three systems at pH range of 5.5–7.0 (for L3 both $[ZnH_3L]^{2+}$ and $[ZnH_2L]^{+}$ complex species and for L2 and L1 in $[ZnH_2L]^{+}$ complex species). ΔE indicates the relative energy of the systems with Zn(II)–L3 being the most stable.

Impact on Zn(II) coordination and peptidomimetic modifications on secondary structure

According to the literature, changing the configuration of amino acids in a peptide sequence from L to D not only

enhances resistance to proteolysis, as D-amino acids are not recognized by common human proteases and thus resist degradation, but also promotes the formation of specific secondary structure.[54] However, in this case, no significant changes were observed in the far-UV circular dichroism (CD) spectra of the studied systems. As shown in Fig. 9A, only at pH 5.4, primarily in the case of the L1 peptide alone and also after the addition of Zn(II) ions to this ligand, were some small tendencies toward PPII helical structure formation present, with characteristic bands observed at 198 nm and 226 nm.[55] A

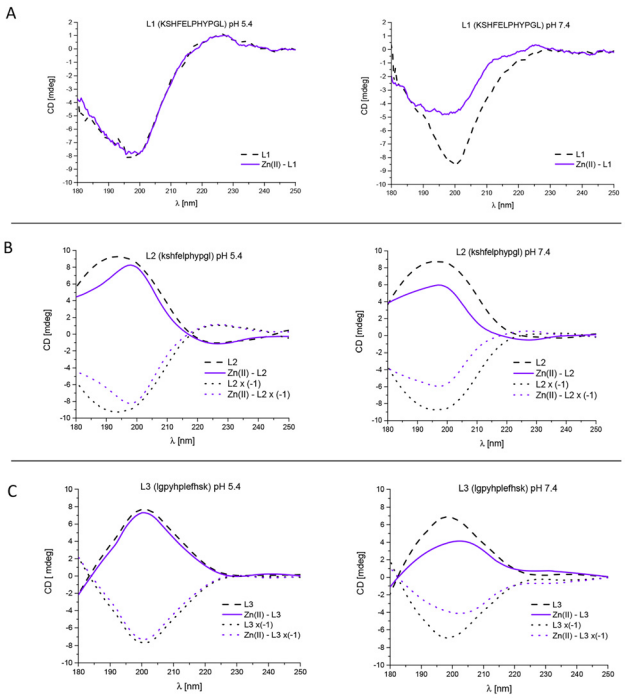

Fig. 9 CD spectra in the far-UV (180–250 nm) region at chosen pH values: 5.4 (left) and 7.4 (right) for the Zn(II) complexes with (A) L1 (KSHFELPHYPGL), (B) L2 (kshfelphypgl) and (C) L3 (lgpyhplefhsk) ligands in aqueous solution of 4 mM $HClO_4$ with I = 0.1 M $NaClO_4$; molar ratio M : L – 0.8 : 1; the optical path length = 0.2 mm; C_L = 0.3 mM; dashed lines correspond to the ligand spectra; dotted lines correspond to recorded spectra with opposite sign for better comparison with the native – L-amino acid peptide.

Ramachandran analysis of the calculated Zn(II)–L1 complex proved however inconclusive, and could not confirm this assumption. The spectrum of the Zn(II)–L2 complex at pH 5.4 may also suggest a partial induction of a polyproline type II helix due to metal ion coordination (Fig. 9B). However, it should be emphasized that experimental studies did not confirm the presence of complexes at pH values below 5.4, making it difficult to unequivocally determine the impact of Zn(II) coordination on this structural change. In most cases, the obtained spectra (and their mirror images for spectra with ligands containing D-amino acids) are similar to that of a random coil, and the addition of metal ions does not significantly alter them. Therefore, it can be concluded that neither peptidomimetic modifications, including the substitution of L-amino acids with D-amino acids and the application of the *retro-inverso* strategy, nor the incorporation of metal ions, induce significant changes in the secondary structures of the Zn(II) complexes with the ligands studied in this work – neither at pH 5.4, nor at pH 7.4.

Impact of Zn(II) coordination and peptidomimetic modifications on antimicrobial activity

A broth microdilution assay was used to evaluate the antimicrobial efficacy of MUC7 peptidomimetics (L1, L2 and L3), and Zn(II) ion complexes by determining the minimum inhibitory concentration (MIC), defined as the lowest concentration that inhibits microbial growth. Given the slightly acidic nature of saliva (pH 5.0 to 8.0), the antimicrobial activity was tested against six bacterial species and *C. albicans* at pH 7.4 (Table 2) and pH 5.4 (Table 3). The results showed that the antimicrobial activity of MUC7-derived peptides, specifically L1, L2, and L3, was enhanced upon coordination with Zn(II) ion. All peptides and their metal complexes were more effective against Gram-positive bacteria, with *S. mutans* being the most susceptible strain (Tables 2 and 3). For *S. mutans* at pH 5.4, the MICs for L1, L2, and L3 were 125 μg mL^{-1}, 250 μg mL^{-1}, and 250 μg mL^{-1}, respectively, while Zn(II)–peptide complexes showed lower MICs: 31.25 μg mL^{-1} for Zn(II)–L1 and 125 μg mL^{-1} for Zn(II)–L2 and Zn(II)–L3. Peptides L1, L2, and L3 also exhibited antifungal activity against *Candida* species, with a 2- to 4-fold increase in activity when bound to Zn(II). Peptidomimetics mimicking MUC7 functional domains

Table 2 The antibacterial and anti-*Candida* activities of peptides/complexes were assessed *in vitro* by determining their MIC (μg mL^{-1}). Antimicrobial tests were conducted in a 10 mM HEPES buffer at pH 7.4. Experiments were performed for peptides and their zinc(II) complexes. n/d, not determined within the concentration range used in this study

	KSHFELPHYPGL (L1)		kshfelphypgl (L2)		lgpyhplefhsk (L3)	
Strain	KSH	+Zn(II)	ksh	+Zn(II)	lgp	+Zn(II)
E. coli ATCC 25922	n/d	n/d	n/d	n/d	n/d	n/d
P. aeruginosa ATCC 15422	n/d	125	n/d	250	n/d	250
S. aureus ATCC 25923	n/d	500	500	250	n/d	500
E. faecalis ATCC 29212	n/d	500	n/d	n/d	n/d	250
S. mutans PCM 2502	125	62.5	500	250	500	250
S. sanguinis PCM 2335	500	250	500	250	500	250
C. albicans SC5314	250	125	n/d	125	500	250

Table 3 The antibacterial and anti-*Candida* activities of peptides/complexes were assessed *in vitro* by determining their MIC (μg mL^{-1}). Antimicrobial tests were conducted in a 10 mM MES buffer at pH 5.4. Experiments were performed for peptides and their zinc(II) complexes. n/d, not determined within the concentration range used in this study

	KSHFELPHYPGL (L1)		kshfelphypgl (L2)		lgpyhplefhsk (L3)	
Strain	KSH	+Zn(II)	ksh	+Zn(II)	lgp	+Zn(II)
E. coli ATCC 25922	n/d	n/d	n/d	n/d	n/d	*n/d*
P. aeruginosa ATCC 15422	n/d	125	500	125	n/d	125
S. aureus ATCC 25923	n/d	250	250	250	n/d	250
E. faecalis ATCC 29212	n/d	500	n/d	n/d	n/d	250
S. mutans PCM 2502	125	31.25	250	125	250	125
S. sanguinis PCM 2335	250	125	500	125	500	250
C. albicans SC5314	125	31.25	250	125	250	125

demonstrated significant antimicrobial activity, especially when coordinated with Zn(II) ion. These results suggest that metal ion coordination improves the antimicrobial effectiveness of these peptides.

Conclusions

MUC7 peptidomimetics, when combined with metal ions such as Zn(II) (and Cu(II) characterized in our previous report[52]), represent a promising avenue for developing new antimicrobial therapies, particularly in the context of rising antibiotic resistance. In our study, we demonstrated that Zn(II) coordination significantly enhances the antimicrobial and antifungal efficacy of the studied peptides. Although the native peptide exhibited the highest activity, the MIC values of the peptidomimetics are also promising, especially considering their greater resistance to proteolytic degradation. From a coordination perspective, we demonstrated that, in addition to exhibiting the same coordination mode at pH 7.4, the *retro-inverso* peptidomimetic displays the highest Zn(II) binding affinity compared to the native peptide and its D-amino acid analogue. However, this is not reflected in enhanced antimicrobial efficacy; therefore, we cannot suggest an antimicrobial mechanism based on 'nutritional immunity'.

As the Zn(II) ion significantly enhances the antimicrobial efficacy, we suggest that the antimicrobial mechanism of these systems is likely associated with the disruption of microbial cell structures and alterations in membrane integrity – a phenomenon supported by previous studies.[23,56] However, to confirm or exclude this hypothesis, further experiments are necessary to gain a precise understanding of the underlying mechanism.

Given the growing threat of multidrug-resistant pathogens, exploring metal–peptide complexes as therapeutic agents offers an innovative approach to tackling this global health challenge. A deeper understanding of how metalloAMPs utilize Zn(II) to enhance antimicrobial activity could pave the way for designing next-generation antimicrobial agents. Future studies should focus on optimizing these complexes and investigating their broader applications in treating both bacterial and fungal infections.

A particularly urgent area for new therapeutic strategies is *Candida* infections, which pose a serious medical concern due to their ability to disseminate to multiple organs and their limited treatment options.[57] *Candida albicans*, a common fungal species within the human microbiota, can transition from a commensal organism to a pathogen under conditions such as microbiota disruption, immunosuppression, or environmental stress, leading to infections ranging from mild mucosal conditions to severe systemic disease.[58,59] Given that antimicrobial peptides combined with Zn(II) exhibit exceptionally high antifungal activity, this combination could serve as a strong candidate for future antifungal drug development.[19]

Overall, our findings emphasize the potential of Zn(II)-coordinated MUC7 peptidomimetics as a foundation for new antimicrobial strategies addressing both bacterial and fungal infections. Our study demonstrates that both D-amino acid and *retro-inverso* analogues of MUC7 fragment retain full antimicrobial activity while being protease resistant, which is an essential advance for therapeutic applications. This is the first systematic evaluation of Zn(II) effects on not only native but also modified analogues, with the *retro-inverso* variant showing the strongest enhancement against *E. faecalis*. This highlights Zn(II) importance beyond native sequences. Lastly, the complementary coordination evaluation is a key modulator of activity, offering new insights into Zn(II)–peptidomimetic interactions – an area previously unexplored. Further research is needed to refine these metal–peptide complexes and unlock their full therapeutic potential.

Author contributions

J. W. – funding acquisition, conceptualization, supervision, validation, writing – review & editing; K.S – investigation, validation, writing – original draft; A. K. – investigation, visualisation, writing – original draft; F. Z. – investigation, visualisation; T. J. – resources, writing – original draft, supervision; D. V. – supervision, validation, writing – review & editing.

Conflicts of interest

There are no conflicts to declare.

Data availability

The data supporting this study, including certificates of analysis of synthesized peptides, MALDI mass spectra of the trypsin digestion experiment, potentiometric titrations, NMR spectroscopic measurements, mass spectrometry results, and DFT calculations, are available in the ESI.† Biological assay data related to antimicrobial activity are provided within the main article and ESI.† No restrictions apply to the availability of these data. If any additional questions regarding experimental details may arise, the corresponding author remain at the Readers' disposal.

Acknowledgements

This work was supported by the National Science Centre (UMO-2021/41/B/ST4/02654 – J. W.). The authors would like to thank the prof. Elżbieta Gumienna-Kontecka from University of Wrocław for kindly providing the Jasco J-1500 CD spectropolarimeter. The authors thank M.Sc. Monika Sabieraj for her support in potentiometric and far-UV CD spectroscopy measurements.

References

1 M. Garvey, *Infect. Dis. Rep.*, 2023, **15**, 454–469.
2 Y. Huan, Q. Kong, H. Mou and H. Yi, *Front. Microbiol.*, 2020, **11**, 582779.
3 J. Mwangi, X. Hao, R. Lai and Z.-Y. Zhang, *Zool. Res.*, 2019, **40**, 488–505.
4 J. Xuan, W. Feng, J. Wang, R. Wang, B. Zhang, L. Bo, Z.-S. Chen, H. Yang and L. Sun, *Drug Resistance Updates*, 2023, **68**, 100954.
5 Q.-Y. Zhang, Z.-B. Yan, Y.-M. Meng, X.-Y. Hong, G. Shao, J.-J. Ma, X.-R. Cheng, J. Liu, J. Kang and C.-Y. Fu, *Mil. Med. Res.*, 2021, **8**, 48.
6 T.-H. Lee, K. N. Hall and M.-I. Aguilar, *Curr. Top. Med. Chem.*, 2015, **16**, 25–39.
7 G. Weiss and P. L. Carver, *Clin. Microbiol. Infect.*, 2018, **24**, 16–23.
8 S. L. Begg, *Biochem. Soc. Trans.*, 2019, **47**, 77–87.
9 W. F. Walkenhorst, J. N. Sundrud and J. M. Laviolette, *Biochim. Biophys. Acta, Biomembr.*, 2014, **1838**, 2234–2242.
10 K. Szarszoń, S. Andrä, T. Janek and J. Wątły, *Inorg. Chem.*, 2024, **63**, 11616–11627.
11 A. Hrdina and I. Iatsenko, *Curr. Opin. Insect Sci.*, 2022, **49**, 71–77.
12 E. Dzień, J. Wątły, A. Hecel, A. Mikołajczyk, A. Matera-Witkiewicz, M. Adrover, M. Barceló-Oliver, A. Domínguez-Martín and M. Rowińska-Żyrek, *Dalton Trans.*, 2024, **53**, 19202–19213.
13 A. Miller, A. Matera-Witkiewicz, A. Mikołajczyk-Tarnawa, A. Kola, M. Wiloch, M. Jonsson-Niedziolka, R. Wieczorek, J. Wątły, D. Valensin and M. Rowińska-Żyrek, *Chem. Sci.*, 2025, **16**, 3447–3458.
14 D. Bellotti, M. D'Accolti, W. Pula, N. Huang, F. Simeliere, E. Caselli, E. Esposito and M. Remelli, *Gels*, 2023, **9**, 165.
15 E. Dzień, J. Wątły, A. Kola, A. Mikołajczyk, A. Miller, A. Matera-Witkiewicz, D. Valensin and M. Rowińska-Żyrek, *Dalton Trans.*, 2024, **53**, 7561–7570.
16 K. Szarszoń, N. Baran, P. Śliwka, M. Wiloch, T. Janek and J. Wątły, *Inorg. Chem.*, 2024, **63**, 19105–19116.
17 D. Łoboda, H. Kozłowski and M. Rowińska-Zyrek, *New J. Chem.*, 2018, **42**, 4560–7568.
18 B. E. Bunnell, J. F. Escobar, K. L. Bair, M. D. Sutton and J. K. Crane, *PLoS One*, 2017, **12**, e0178303.
19 C. Donaghy, J. G. Javellana, Y.-J. Hong, K. Djoko and A. M. Angeles-Boza, *Molecules*, 2023, **28**, 2156.
20 J. Wątły, K. Szarszoń, A. Mikołajczyk, M. Grelich-Mucha, A. Matera-Witkiewicz, J. Olesiak-Bańska and M. Rowińska-Żyrek, *Inorg. Chem.*, 2023, **62**, 19786–19794.
21 D. Dudek, E. Dzień, J. Wątły, A. Matera-Witkiewicz, A. Mikołajczyk, A. Hajda, J. Olesiak-Bańska and M. Rowińska-Żyrek, *Sci. Rep.*, 2022, **12**, 20543.
22 J. X. Campbell, S. Gao, K. S. Anand and K. J. Franz, *ACS Infect. Dis.*, 2022, **8**, 1920–1934.
23 S. S. Duay, G. Sharma, R. Prabhakar, A. M. Angeles-Boza and E. R. May, *J. Phys. Chem. B*, 2019, **123**, 3163–3176.
24 S. A. Juliano, L. F. Serafim, S. S. Duay, M. Heredia Chavez, G. Sharma, M. Rooney, F. Comert, S. Pierce, A. Radulescu, M. L. Cotten, M. Mihailescu, E. R. May, A. I. Greenwood, R. Prabhakar and A. M. Angeles-Boza, *ACS Infect. Dis.*, 2020, **6**, 1250–1263.
25 A. M. Martini, B. S. Moricz, A. K. Ripperger, P. M. Tran, M. E. Sharp, A. N. Forsythe, K. Kulhankova, W. Salgado-Pabón and B. D. Jones, *Front. Microbiol.*, 2020, **11**, 10.
26 C. Bales, J. Freeland-Graves, S. Askey, F. Behmardi, R. Pobocik, J. Fickel and P. Greenlee, *Am. J. Clin. Nutr.*, 1990, **51**, 462–469.
27 A. Janicka-Kłos, T. Janek, J. Burger and H. Czapor-Irzabek, *J. Inorg. Biochem.*, 2020, **203**, 110923.
28 A. Marr, W. Gooderham and R. Hancock, *Curr. Opin. Pharmacol.*, 2006, **6**, 468–472.
29 J. Wątły, A. Miller, H. Kozłowski and M. Rowińska-Żyrek, *J. Inorg. Biochem.*, 2021, **217**, 111386.
30 Z. Feng and B. Xu, *Biomol. Concepts*, 2016, **7**, 179–187.
31 M. Garton, S. Nim, T. A. Stone, K. E. Wang, C. M. Deber and P. M. Kim, *Proc. Natl. Acad. Sci. U. S. A.*, 2018, **115**, 1505–1510.
32 K. Hamamoto, Y. Kida, Y. Zhang, T. Shimizu and K. Kuwano, *Microbiol. Immunol.*, 2002, **46**, 741–749.
33 L. Gentilucci, R. De Marco and L. Cerisoli, *Curr. Pharm. Des.*, 2010, **16**, 3185–3203.
34 N. Doti, M. Mardirossian, A. Sandomenico, M. Ruvo and A. Caporale, *Int. J. Mol. Sci.*, 2021, **22**, 8677.
35 J. Rai, *Chem. Biol. Drug Des.*, 2019, **93**, 724–736.
36 M. H. Cardoso, E. S. Cândido, K. G. N. Oshiro, S. B. Rezende and O. L. Franco, *Pept. Appl. Biomed., Biotechnol. Bioeng.*, 2018, pp. 131–155.
37 P. Gans, *Talanta*, 2000, **51**, 33–37.

38 G. Gran, H. Dahlenborg, S. Laurell and M. Rottenberg, *Acta Chem. Scand.*, 1950, **4**, 559–577.
39 P. Gans, A. Sabatini and A. Vacca, *Talanta*, 1996, **43**, 1739–1753.
40 Ch. F. Baes and R. E. Mesmer, *The Hydrolysis of Cations*, Wiley, New York, 1976, p. 293.
41 L. Alderighi, P. Gans, A. Ienco, D. Peters, A. Sabatini and A. Vacca, *Coord. Chem. Rev.*, 1999, **184**, 311–318.
42 P. J. Stephens, F. J. Devlin, C. F. Chabalowski and M. J. Frisch, *J. Phys. Chem.*, 1994, **98**, 11623–11627.
43 A. D. Becke, *J. Chem. Phys.*, 1993, **98**, 5648–5652.
44 A. M. Gillum, E. Y. H. Tsay and D. R. Kirsch, *Mol. Gen. Genet.*, 1984, **198**, 179–182.
45 I. Wiegand, K. Hilpert and R. E. W. Hancock, *Nat. Protoc.*, 2008, **3**, 163–175.
46 P. Potok, M. Zawada and S. Potocki, *J. Inorg. Biochem.*, 2024, **253**, 112500.
47 V. Dzyhovskyi and K. Stokowa-Sołtys, *J. Inorg. Biochem.*, 2023, **244**, 112203.
48 D. Dudek, A. Miller, A. Hecel, A. Kola, D. Valensin, A. Mikołajczyk, M. Barcelo-Oliver, A. Matera-Witkiewicz and M. Rowińska-Żyrek, *Inorg. Chem.*, 2023, **62**, 14103–14115.
49 J. Wątły, A. Hecel, M. Rowińska-Żyrek and H. Kozłowski, *Inorg. Chim. Acta*, 2018, **472**, 119–126.
50 M. Remelli, D. Brasili, R. Guerrini, F. Pontecchiani, S. Potocki, M. Rowinska-Zyrek, J. Watly and H. Kozlowski, *Inorg. Chim. Acta*, 2018, **472**, 149–156.
51 D. Bellotti, C. Tocchio, R. Guerrini, M. Rowińska-Żyrek and M. Remelli, *Metallomics*, 2019, **11**, 1988–1998.
52 J. Wątły, K. Szarszoń, M. Sabieraj, A. Kola, R. Wieczorek, T. Janek and D. Valensin, *Inorg. Chem.*, 2025, **64**, 6365–6377.
53 S. Ben-Shushan, A. Hecel, M. Rowinska-Zyrek, H. Kozlowski and Y. Miller, *Inorg. Chem.*, 2020, **59**, 925–929.
54 S. Y. Hong, J. E. Oh and K.-H. Lee, *Biochem. Pharmacol.*, 1999, **58**, 1775–1780.
55 A. L. Rucker and T. P. Creamer, *Protein Sci.*, 2002, **11**, 980–985.
56 H. L. Norris, R. Kumar, C. Y. Ong, D. Xu and M. Edgerton, *J. Fungi*, 2020, **6**, 124.
57 J. Kaur and C. J. Nobile, *Curr. Opin. Microbiol.*, 2023, **71**, 102237.
58 D. Agustina, R. T. Chrisnawati, B. E. Chrismawaty, S. B. Wongsohardjono, F. Naritasari and A. Sarasati, *Maj. Kedokt.*, 2023, **9**, 57.
59 C. A. Kumamoto, M. S. Gresnigt and B. Hube, *Curr. Opin. Microbiol.*, 2020, **56**, 7–15.